



# Insight on corrosion behavior of a Cu–P–Cr–Ni steel with different Ni contents by electrochemical and periodic immersion corrosion experiments

Zhi-wei Lian<sup>1</sup> · Tian-en Peng<sup>1</sup> · Shuang Hu<sup>1</sup> · Bo He<sup>2</sup> · Xue-wen Hu<sup>2</sup> · Tao Zhu<sup>2</sup> · Bo Jiang<sup>1</sup>

Received: 12 January 2022 / Revised: 19 February 2022 / Accepted: 9 March 2022 / Published online: 6 April 2022  
© China Iron and Steel Research Institute Group 2022

## Abstract

Corrosion behavior of Cu–P–Cr–Ni weathering steels with different nickel contents was studied by periodic immersion corrosion test for 72 h. The mass loss method was used to evaluate the weatherability of weathering steel. The rust layers formed on weathering steel were characterized by scanning electron microscopy, X-ray diffraction, electron probe microanalysis, X-ray photoelectron spectroscopy, and electrochemical measurements. The results of periodic immersion corrosion test for 72 h showed that the mass loss rates of Cu–P–Cr–0.14Ni steel and Cu–P–Cr–0.04Ni steel were 1.57 and 1.61 g/(m<sup>2</sup> h), respectively. According to the electrochemical experiment, the corrosion potentials of the two tested steels at the initial stage of corrosion were – 0.6852 and – 0.7037 V, respectively. With the corrosion time reaching 72 h, the corrosion potential difference between the two tested steels was gradually reduced. In the initial stage, NiO was formed in the rust layer and can dramatically promote the crystallization of corrosion products to improve the stability of the rust layer. After periodic immersion corrosion test for 72 h, Ni element had no obvious effect. At this time, it was mainly the enrichment of Cu and Cr elements in the form of CuO and Cr<sub>2</sub>O<sub>3</sub> in the rust layer that could further protect the matrix.

**Keywords** Weathering steel · Ni · Electrochemical experiment · Periodic immersion corrosion · Corrosion behavior

## 1 Introduction

The weathering steel has been widely used in different areas of life, like bridge, construction industry, transportation, container fields, and so on. It has been known that container transport is a modern and efficient transport way. However, the container has been facing severe atmospheric corrosion due to its long-time corrosive conditions [1–4]. Therefore, higher corrosion resistance has been always required for the weathering steel for container.

Many researchers have developed a series of weathering steels by adding alloying elements like copper, chromium, and nickel to carbon steel [5–9]. These alloying elements

can improve the protection ability of rust layer and isolate steel from various corrosion media, thus greatly reducing the corrosion rate [10]. There have been a lot of studies focused on the anti-corrosion mechanisms of alloying elements. Kimura et al. [11] concluded that the presence of nickel in Cu–P–Cr–3.0Ni steel modified the surface charge of the rust, preventing chloride ions from reaching the steel surface in a marine atmosphere. Similar to nickel, chromium also has a significant effect on corrosion resistance. Qian et al. [12] pointed out that the beneficial effect of alloyed chromium was attributed to both its promotion to the formation of a protective rust layer that acted as a barrier against corrosion process, and its enhancement of passivation capability that decreased the anodic dissolution of substrate alloys. Qian et al. [12] also suggested that the higher the content of Cr was, the more obvious the beneficial effect was. In addition, Zhang et al. [13] and Li et al. [14] found that in iron hydroxide compounds, Cr partially replaced Fe in Cu–P–1.53Cr steel to form  $\alpha$ -Fe<sub>x</sub>Cr<sub>1-x</sub>OOH, and Cr would precipitate at the defects and grain boundaries of rust layer, filling defects, promoting the formation

✉ Bo Jiang  
jiangbo@ustb.edu.cn

<sup>1</sup> School of Materials Science and Engineering, University of Science and Technology Beijing, Beijing 100083, China

<sup>2</sup> Technical Center, Ma'anshan Iron & Steel Co., Ltd., Ma'anshan 243041, Anhui, China

of dense and stable rust layer, especially the formation of dense internal rust layer, inhibiting corrosive medium from reaching the surface of steel matrix and improving the corrosion resistance of steel in marine atmosphere. However, Cr was usually added together with Cu in weathering steels rather than alone. Cu and Cr were enriched in the rust layer after the combined addition [15]. The synergistic effect of the two alloying elements enhanced the protective effect of the rust layer.

The improvement of corrosion resistance mainly depended on the addition of alloying elements such as Cu, P, Cr, and Ni. Among the commonly used alloying elements, e.g., Cu, Cr, Ni, and Mo, 3.5 wt.% Ni exhibited the best overall performance [16–20]. Increasing the amount of alloying elements will inevitably lead to an increase in cost, especially the addition of Ni. Therefore, the preferred way to save costs was to reduce the addition of Ni. There were a lot of researches on the anti-corrosion mechanism of Ni, but the researches mainly focused on the anti-corrosion mechanism of Ni element with medium or higher content. Wu et al. [21] pointed out that 0.5 wt.% Ni participated in the formation of corrosion products, which was enriched in the inner rust layer and promoted the transformation from loose  $\gamma$ -FeOOH to dense  $\alpha$ -FeOOH. Nishimura et al. [22] pointed out that Ni (1–3 wt.%) conduced to the formation of spinel oxides in the rust and helped to convert spinel oxides into a compact and fine structure, which brought about a more protective rust layer on weathering steel. However, when the nickel content exceeded 4 wt.%, the anti-corrosion mechanism of nickel changed. Chen et al. [23] pointed out that the addition of 4.0 wt.% Ni in weathering steel could not only promote the formation process of  $\alpha$ -FeOOH, but also produce a cation-selectivity in the inner rust layer. Some researchers also have tried to further reduce Ni content in the weathering steel to save costs. Song et al. [24] pointed out that in the presence of  $\text{Cl}^-$ , when the mass fraction of nickel is less than 0.25 wt.%, it does not play a leading role in the corrosion resistance. There are similar results in the atmospheric environment. Zhu et al. [25] concluded that the low content of Ni in the alloy has little effect on the corrosion resistance of 09CuPCrNi steel by reducing the mass fraction of Ni in 09CuPCrNi steel from 0.160 to 0.115 wt.%. At present, the production cost of weathering steel was still high. Therefore, it was necessary to consider further reducing the addition of Ni. However, there was a lack of in-depth study on the effect and mechanism of weathering steel with Ni content below 0.1 wt.% in industrial atmosphere.

The present study focused on the corrosion behavior in industrial atmosphere of a low-carbon Cu–P–Cr–Ni high-strength weathering steel. The effect of Ni above 0.1 wt.% and below 0.1 wt.% in industrial atmosphere was studied by periodic immersion corrosion test. The anti-corrosion

mechanism of Ni above 0.1 wt.% and below 0.1 wt.% was discussed by means of electrochemical experiment, microstructure, phase composition analysis and thermodynamic calculation. Further, the present study lays a theoretical foundation for the development of the high-strength low-nickel weathering steel.

## 2 Experimental

### 2.1 Materials

The billets of the investigated weathering steel with different compositions were smelted and forged into 60 mm × 150 mm × 200 mm slabs. The slabs were rolled into an intermediate slab of 20 mm × 180 mm × 500 mm by simulating rough rolling deformation in a rolling mill. The heating temperature was 1250 °C and final rolling temperature was 1050 °C. Then, the intermediate slabs were rolled into a steel plate of 6 mm × 180 mm × 600 mm with the final rolling temperature of 900 °C. The steel plate was cooled by laminar flow after the final rolling and then put into a 620 °C heating furnace to simulate coiling. The chemical compositions of the two tested steels used in the experiments are given in Table 1. The main difference was Ni content. The nickel content of the two experimental steels was higher than 0.1 wt.% and lower than 0.1 wt.%, respectively. It was used to study the influence of Ni element on corrosion resistance. Both the structure of tested steels was ferrite–pearlite, and the grain size and phase ratio were similar.

### 2.2 Experimental method

The steel plate was machined into the standard size to carry out the periodic immersion accelerated corrosion test. Three parallel specimens of each steel were prepared with the dimensions of 60 mm × 40 mm × 5 mm. The specimens were drilled, dehydrated with alcohol, and deoiled with acetone before the test. Then, the specimens were numbered and weighed, and the external dimensions were measured for use. Periodic immersion corrosion test for 72 h was carried out in an LF-65A periodic round immersion corrosion test chamber according to the standard TB/T2375-93. The specimens were immersed into 0.01 mol/L  $\text{NaHSO}_3$  aqueous solution at 45 °C for 12 min, and then, the specimens were dried immediately after immersion. The surface temperature of the specimens was lower than 80 °C. Subsequently, the specimens were held in the testing chamber with a constant humidity of relative humidity 70% at 45 °C for 48 min totally. The corrosion products covering on the specimens were removed by a descaling liquid consisting of 500 mL HCl, 500 mL  $\text{H}_2\text{O}$ ,

**Table 1** Chemical composition of tested steels (wt.%)

Steel	C	Si	Mn	P	S	Al	Cu	Cr	Ni	Ti	Fe
Cu-P-Cr-0.14Ni	0.076	0.47	0.49	0.023	0.006	0.019	0.25	0.45	0.14	0.052	Balance
Cu-P-Cr-0.04Ni	0.067	0.45	0.53	0.025	0.006	0.020	0.26	0.45	0.04	0.057	Balance

and 3.5 g hexamethylenetetramine in an ultrasonic apparatus. After cleaning, the rust layer was washed with water and alcohol in turn and weighed. The mass loss rate was calculated according to the following equation.

$$W = \frac{(m_0 - m_1) \times 10^6}{(S \cdot t)} \quad (1)$$

where  $W$  is the mass loss rate,  $\text{g}/(\text{m}^2 \text{ h})$ ;  $m_0$  and  $m_1$  are the mass of the specimen before and after corrosion test, respectively, g;  $S$  is the corrosion surface area,  $\text{mm}^2$ ; and  $t$  is the experiment time, h.

Surface morphologies and cross-sectional morphologies of the two steels were observed with a camera and a Gemini 500 field emission scanning electron microscope. Element distribution and phase compositions of the corrosion products were analyzed by JEOL JXA-8100 electron probe and X-ray diffraction (XRD). X-ray photoelectron spectroscopy (XPS) experiment was carried out by using AXIS ULTRA<sup>DLD</sup> system. The excitation source was Al  $K\alpha$  radiation (photoelectron energy = 1486.6 eV). The spectra were analyzed using XPSPEAK 4.0 software according to the database [26]. The absolute binding energies of different surface species were calibrated using C 1s line at 284.8 eV.

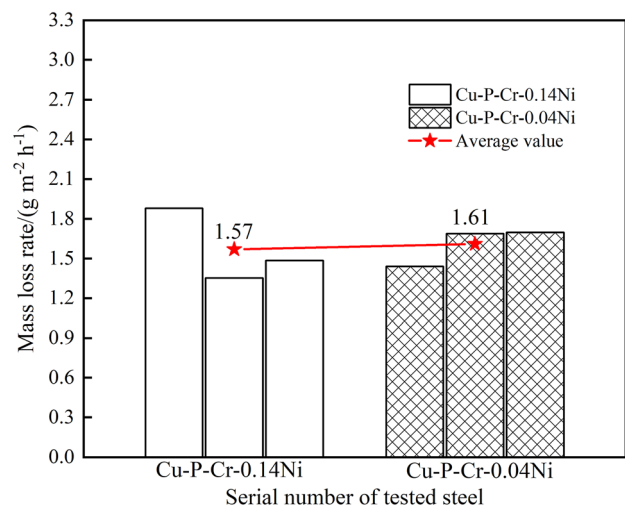
The steel plate with the size of 10 mm × 10 mm × 5 mm was used for the electrochemical experiment of bare steel. In addition, the steel plate with the same size was taken from the periodic immersion corrosion specimen for the electrochemical experiment to study the corrosion resistance. Notably, the periodic immersion corrosion specimen with the mass loss rate closest to the average mass loss rate was selected for electrochemical experiments. In fact, the surface of bare steel specimen has been slightly corroded. The corrosion time was very short compared to 72 h periodic immersion corrosion time; thus, the bare steel specimen was being corroded in the early stage of corrosion. The electrochemical measurements were conducted in a conventional three-electrode cell with a Pt plate as a counter electrode and a saturated calomel electrode (SCE) as a reference electrode in a 0.01 mol/L  $\text{NaHSO}_3$  solution. The temperature of  $\text{NaHSO}_3$  solution was kept at 25 °C. The surfaces of the specimen were degreased with acetone and dried. The as-prepared and rusted steel specimens were employed as working

electrodes with an exposed area of 1  $\text{cm}^2$ . The frequency range for electrochemical impedance spectroscopy (EIS) was from  $10^5$  to  $10^{-2}$  Hz. The polarization curves were obtained at a constant scan rate of 20 mV/min. The obtained experimental data were analyzed by using the ZSimpWin software [27].

### 3 Results and discussion

#### 3.1 Corrosion resistance and analysis of rust layer

The statistical results of mass loss rate after periodic immersion corrosion test for 72 h are shown in Fig. 1. The mass loss rates of the two tested steels were 1.57 and 1.61  $\text{g}/(\text{m}^2 \text{ h})$ , respectively. The result shows that there was little difference in the corrosion resistance of the two tested steels after periodic immersion corrosion test for 72 h. Cross-sectional morphologies of the rust layer and distribution of elements on two steels are shown in Fig. 2. It can be seen from Fig. 2 that the surface rust layers of the two weathering steels were stratified, showing inner rust layer and outer rust layer. The inner rust layer of the two tested steels was relatively dense and the connection between substrate and inner rust layer was fine. The inner rust layer thickness ranged from 20 to 60  $\mu\text{m}$ . The continuous inner

**Fig. 1** Mass loss rate of different tested steels

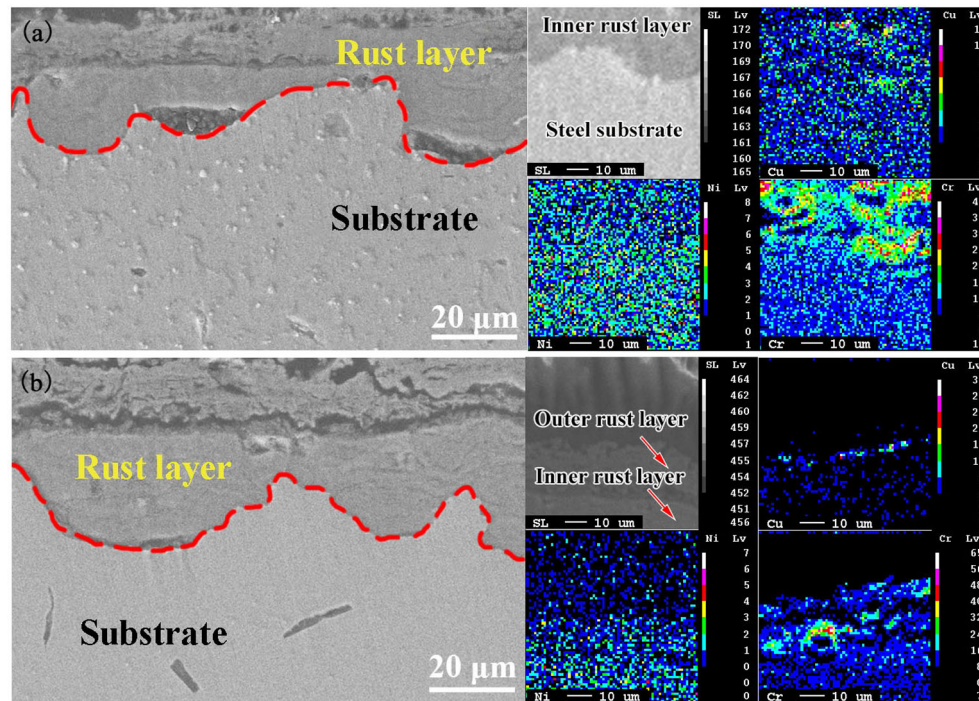


**Fig. 2** Field emission scanning electron microscopy (SEM) and electron probe microanalysis (EPMA) of surface scanning composition of longitudinal sections of two tested steels after periodic immersion corrosion test for 72 h. **a** Cu–P–Cr–0.14Ni steel; **b** Cu–P–Cr–0.04Ni steel

rust layer helped prevent the diffusion of  $O_2$  into the substrate [28]. The outer rust layer was loose with a thickness ranging from 10 to 15  $\mu\text{m}$ . During the corrosion process of the tested steel, the iron on the surface first dissolved. A loose and porous outer rust layer was formed. The corrosion medium in the environment passed through the outer rust layer and reached the surface of the substrate for further corrosion [29]. The protection ability of the rust layer on the substrate was affected by the compactness of the rust layer greatly. Previous studies have shown that the rust layer of weathering steel consists of inner rust layer and outer rust layer [30]. In general, the rust layers of the two weathering steels were compact and flat, which had a strong protective effect on the substrate. They could hinder the contact between the corrosion medium and the steel substrate in the environment [30–32]. The distribution of elements in the inner rust layer is of great significance to the study of its mechanism. Studies pointed out that the enrichment of Cu in the rust layer will enhance the protection and densification of rust [33]. According to previous studies, chromium and copper are mainly concentrated in the inner rust layer, while the outer rust layer is chromium-depleted [34]. It can be seen from Fig. 2 that Ni element was evenly distributed in rust layer after periodic immersion corrosion test for 72 h. However, Cu and Cr elements were enriched in the inner rust layer. Because the observation areas shown in Fig. 2 were different and the enrichment degree was uneven, the enrichment conditions

of Cu and Cr elements with the same content were not completely consistent.

### 3.2 Morphology observation and phase analysis of rust layer

SEM micrographs and X-ray diffraction phase composition of two tested steels after periodic immersion corrosion test for 72 h are shown in Fig. 3. The rust layer of the two tested steels was mainly composed of the rust bubble and the rust matrix as shown in Fig. 3b and h. The rust bubble diameter ranged from 50 to 100  $\mu\text{m}$ . The rust bubbles and rust layer matrix were mainly spherical aggregated iron oxides as shown in Fig. 3e. Studies have shown that the spherical iron oxide is mainly  $\gamma\text{-FeOOH}$  [21]. It can be seen that the uniformity of corrosion products of the two tested steels was similar. This was one of the reasons why there was little difference in mass loss rate between the two tested steels.

Semi-quantitative analysis percentage of XRD after periodic immersion corrosion test for 72 h is shown in Table 2. Kamimura et al. [35] pointed out that the ratio of  $\alpha$  and  $\gamma^*$  content in the rust layer was an important indicator of the stability of the rust layer. The larger the ratio was, the better the protection of the rust layer was.  $\alpha$  refers to  $\alpha\text{-FeOOH}$ , and  $\gamma^*$  refers to the sum of  $\gamma\text{-FeOOH}$ ,  $\beta\text{-FeOOH}$ , and  $\text{Fe}_3\text{O}_4$ . It can be seen from Fig. 3 that the corrosion products of the two tested steels were mainly composed of

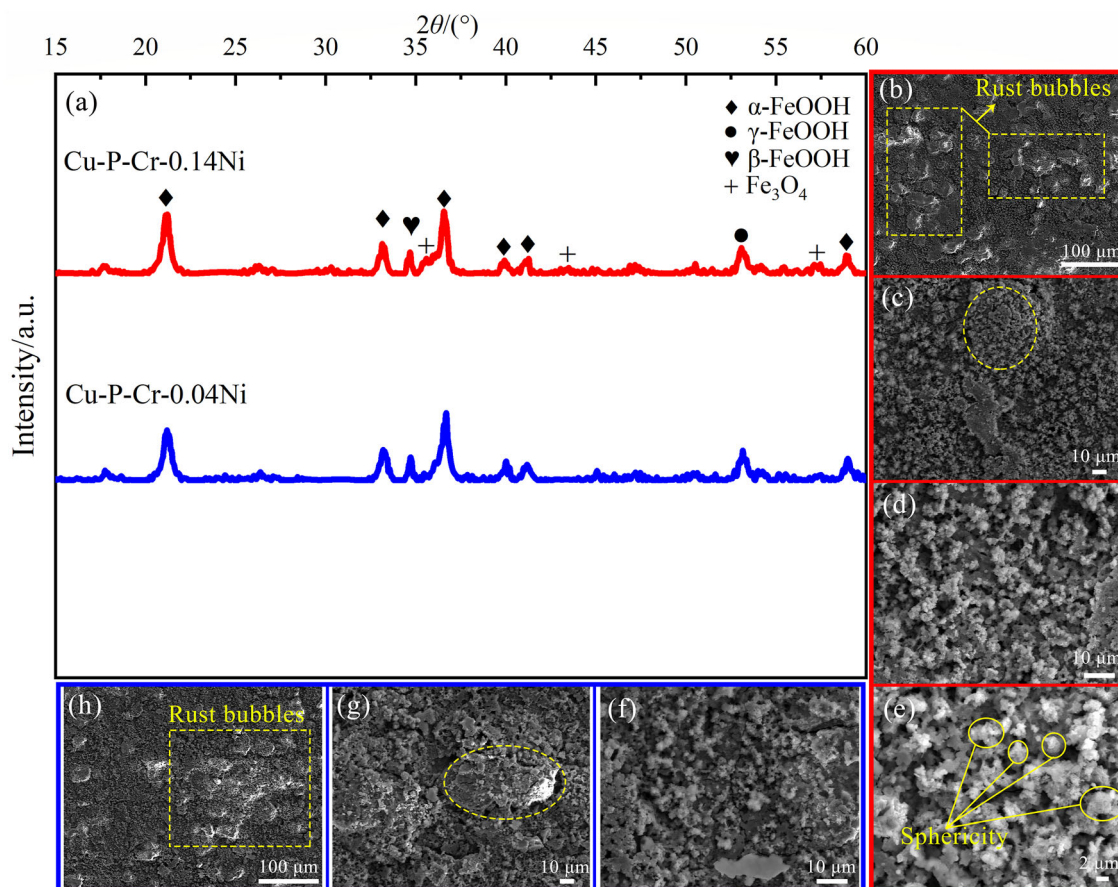


**Fig. 3** X-ray diffraction phase composition (a) and SEM micrographs (b–h) of two tested steels after periodic immersion corrosion test for 72 h. **b–e** Cu–P–Cr–0.14Ni steel, **f–h** Cu–P–Cr–0.04Ni steel

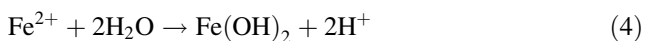
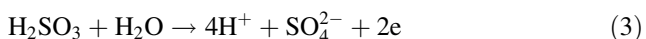
**Table 2** Semi-quantitative analysis percentage of XRD after periodic immersion corrosion test for 72 h

Steel	Proportion of each phase/%				$\alpha/\gamma^*$
	$\alpha$ -FeOOH	$\gamma$ -FeOOH	$\beta$ -FeOOH	$\text{Fe}_3\text{O}_4$	
Cu–P–Cr–0.14Ni	60.43	31.93	3.76	3.88	1.53
Cu–P–Cr–0.04Ni	60.88	35.24	3.88	–	1.56

$\alpha$ -FeOOH,  $\gamma$ -FeOOH, and  $\beta$ -FeOOH. Studies have pointed out that there were  $\alpha$ -FeOOH and  $\gamma$ -FeOOH in rust [36]. It was consistent with XRD results in this experiment.

The following were reactions that occurred in corrosion process [37, 38]:

Anodic reaction [13]



Cathodic reaction



It was worth noting that FeOOH content and  $\text{Fe}_3\text{O}_4$  content in the rust layer of the two tested steels were quite different.  $\gamma$ -FeOOH was the initial phase in the formation of rust layer. Previous study [17] has shown that the addition of Ni can accelerate the nucleation process and retard the growth process of the rust layer.  $\gamma$ -FeOOH was promoted to form rapidly due to the addition of Ni in Cu–P–Cr–0.14Ni steel. According to the above reaction equation, it can be seen that  $\gamma$ -FeOOH was converted into  $\text{Fe}_3\text{O}_4$  in the cathode reaction. It led to the decrease in  $\gamma$ -FeOOH and the increase in  $\text{Fe}_3\text{O}_4$  in Cu–P–Cr–0.14Ni

steel. Therefore, the content of  $\gamma$ -FeOOH in Cu–P–Cr–0.14Ni steel was lower than that in Cu–P–Cr–0.04Ni steel, while the content of Fe<sub>3</sub>O<sub>4</sub> was higher. The proportion of  $\alpha$ -FeOOH was the highest, reaching more than 60%.  $\alpha$ -FeOOH was the most thermodynamically stable and had a very high impedance to slow electron migration. The content of  $\alpha$ -FeOOH determined the stability of rust layer. It can be seen from Table 2 that the content of  $\alpha$ -FeOOH and the ratio of  $\alpha/\gamma^*$  in the two tested steels had very little difference. The results show that the impedance values of the rust layers of the two tested steels should be similar. And then, the stability of the rust layers was similar. Moreover, the results of XRD were in good accordance with mass loss rate in Fig. 1.

### 3.3 XPS analysis of rust layer

Ni typically exists in + 2 valence state in NiO or NiFe<sub>2</sub>O<sub>4</sub> spinel in the rust. When Ni content is very low ( $\sim 0.20$  wt.%), NiFe<sub>2</sub>O<sub>4</sub> spinel product will not be formed [38]. Figure 4a–c shows XPS analysis results of Ni, Cr, and Cu

elements on the rust of the tested steel after periodic immersion corrosion test for 72 h, respectively. Ni 2p<sub>3/2</sub> peak around 853.5 eV indicated the bivalent state of NiO in Cu–P–Cr–0.04Ni steel and it had a satellite peak as shown in Fig. 4a. Ni 2p<sub>3/2</sub> peak around 855.5 eV indicated the bivalent state of NiO in Cu–P–Cr–0.14Ni steel and it had a satellite peak as shown in Fig. 4a. Zhao et al. [30] studied the corrosion behavior of Cu–P–Cr–0.18Ni steels and pointed out that Ni 2p<sub>3/2</sub> peaks around (855.6  $\pm$  0.1) eV and (861.4  $\pm$  0.1) eV indicated the divalent state of NiFe<sub>2</sub>O<sub>4</sub> and trivalent state of Ni<sub>2</sub>O<sub>3</sub>, respectively. However, NiFe<sub>2</sub>O<sub>4</sub> was not detected in this study. Cr 2p<sub>3/2</sub> peak around 576 eV indicated the bivalent state of Cr<sub>2</sub>O<sub>3</sub> as shown in Fig. 4b. Cu 2p<sub>3/2</sub> peak around 933 eV indicated the bivalent state of CuO as shown in Fig. 4c and it had a satellite peak. Choi et al. [39] pointed out in XPS experimental results that in the case of Cr–Cu–0.15Ni steel, chromium oxide (Cr<sub>2</sub>O<sub>3</sub>) and cupric oxide (CuO) were in the rust. This conclusion was completely consistent with the results of this study. Cu and Cr contents of the two steels were similar. The surfaces of the two steels were in

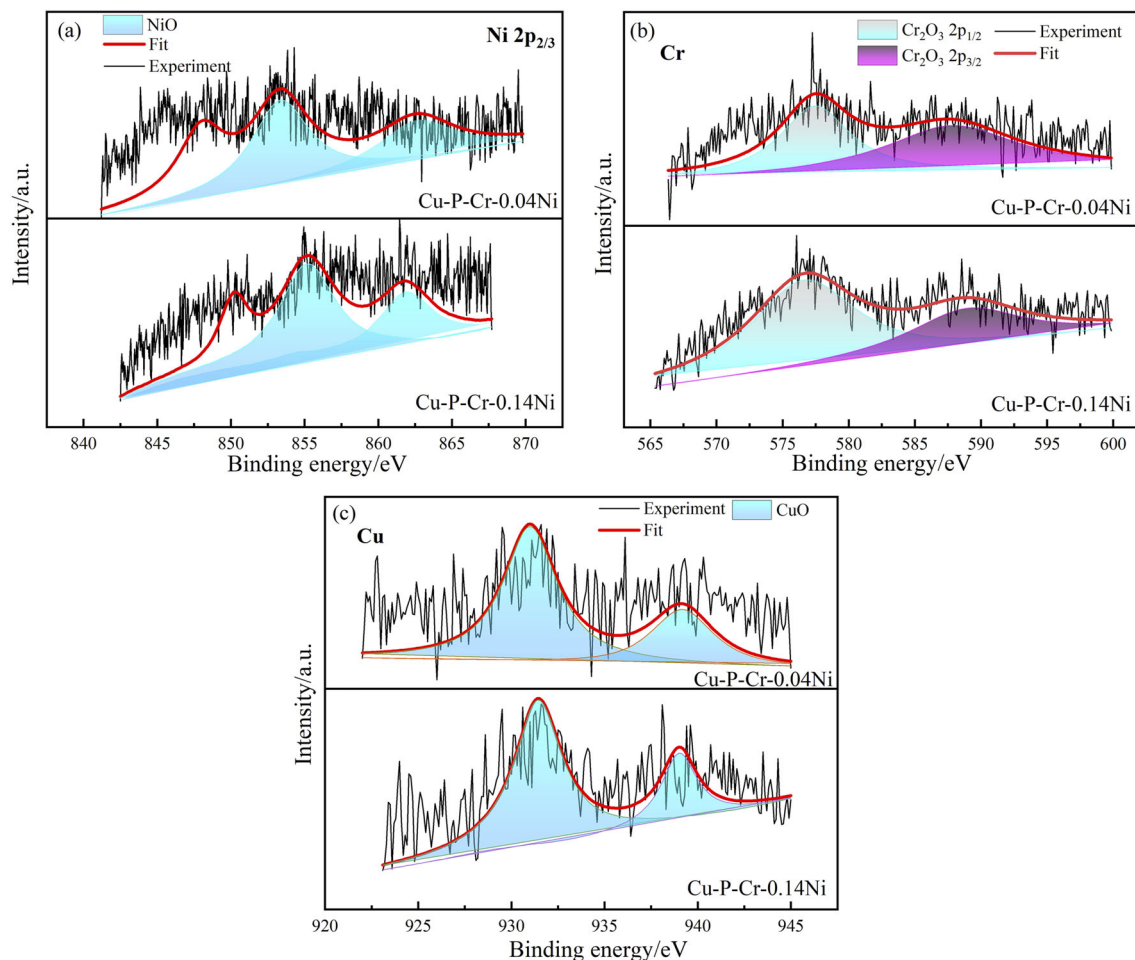


**Fig. 4** Spectra of alloying elements from rust of specimens obtained by XPS after periodic immersion corrosion test for 72 h. **a** Ni; **b** Cr; **c** Cu

contact with air and water for oxidation reaction in corrosive environment, so that the corresponding oxides of copper and chromium produced in the two steels had similar effects.

### 3.4 Electrochemical polarization curve analysis

The tendency of electrochemical corrosion of specimens was characterized by corrosion potential. The lower the corrosion potential, the greater the tendency of electrochemical corrosion. Figure 5 shows the polarization curves of two tested steels where  $E_{\text{corr}}$  represents the corrosion potential, and  $I_{\text{corr}}$  represents the corrosion current density. By comparing the two bare steels in Table 3, it can be found that the corrosion potential of Cu–P–Cr–0.14Ni steel was higher. The result indicated that the addition of Ni (0.14 wt.%) could improve the electrode potential of steel substrate at the initial stage of corrosion. And then, it can make the corrosion more stable and facilitate the formation of dense rust layer.

The cathode polarization of bare steel was controlled by the diffusion of dissolved oxygen, while the anode polarization was controlled by activation polarization. Along with the corrosion time prolonging, the diffusion reaction of dissolved oxygen at cathode had gradually shifted to the reduction of rust layer. Comparing the polarization curves of the two tested steels before and after corrosion, it can be found that the corrosion potential of two tested steels after periodic immersion corrosion test for 72 h had an upward shift compared with that of bare steels. The result also shows that the dissolution reaction of the steel matrix at the anode was inhibited by rust layer formed on the steel surface. At the same time, it can be found that the corrosion potentials of the two tested steels had little difference after

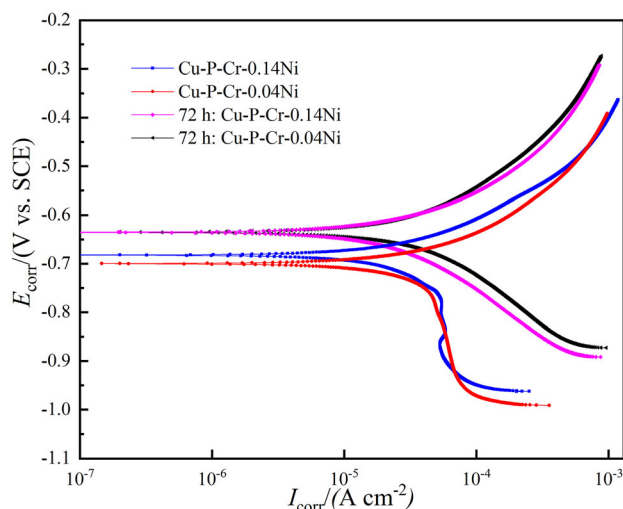


**Fig. 5** Polarization curve of bare steel and tested steel after periodic immersion corrosion test for 72 h

**Table 3** Polarization curve fitting results of specimens

Steel	$E_{\text{corr}}/V$	$I_{\text{corr}}/(A\text{ cm}^{-2})$
Cu–P–Cr–0.14Ni	– 0.6852	$2.8967 \times 10^{-5}$
Cu–P–Cr–0.04Ni	– 0.7037	$3.7705 \times 10^{-5}$
72 h: Cu–P–Cr–0.14Ni	– 0.6380	$2.0187 \times 10^{-5}$
72 h: Cu–P–Cr–0.04Ni	– 0.6370	$2.1316 \times 10^{-5}$

periodic immersion corrosion test for 72 h, indicating that the addition of Ni (0.14 wt.%) did not significantly change the corrosion potential of the tested steel after periodic immersion corrosion test for 72 h.

### 3.5 Electrochemical impedance spectroscopy analysis

Electrochemical impedance spectroscopy can analyze the corrosion mechanism of weathering steel and measure the resistance of corrosion products [40, 41]. The Nyquist plots of two bare steels are shown in Fig. 6a. It can be seen from Fig. 6a that the Nyquist plots of the two bare steels consisted of an incomplete semicircular arc in the high-frequency region and a line representing diffusion in the low-frequency region. The diameter of the arc can be regarded as a charge transfer resistance, while the low-frequency oblique line was related to the diffusion process near the interface. The equivalent electrical circuit (as shown in Fig. 6b) is proposed to simulate the electrochemical process of the bare steel tested in the laboratory. The equivalent circuit model included solution resistance ( $R_s$ ), charge transfer resistance ( $R_{\text{ct1}}$ ,  $R_{\text{ct2}}$ ), the film (mainly the rust layer) capacitance ( $Q_1$ ,  $Q_2$ ), and Warburg impedance ( $R_w$ ).  $Q_1$  was electric double-layer capacitance composed of rust layer and solution, and  $Q_2$  was electric double-layer capacitance composed of metal matrix and infiltrated electrolyte. The Bode plots and phase angle plots of two bare steels are shown in Fig. 6b.  $|Z|$  was used to represent the impedance value. It can be seen from Fig. 6b that the phase angle value of Cu–P–Cr–0.14Ni steel was larger than that of Cu–P–Cr–0.04Ni steel. The fitting results of parameters in equivalent circuit of bare steel are shown in Table 4.  $n$  was used to represent the dispersion effect index. It can be seen from Table 4 that the charge transfer resistance of Cu–P–Cr–0.14Ni steel was greater than that of Cu–P–Cr–0.04Ni steel. The result shows that the electrochemical reaction resistance of Cu–P–Cr–0.14Ni steel was larger, indicating that the ion transport efficiency in the solution cannot meet the needs of rapid electrochemical reaction. Figure 6b shows the result of the Bode plots of the bare steel tested. Usually, the impedance value at

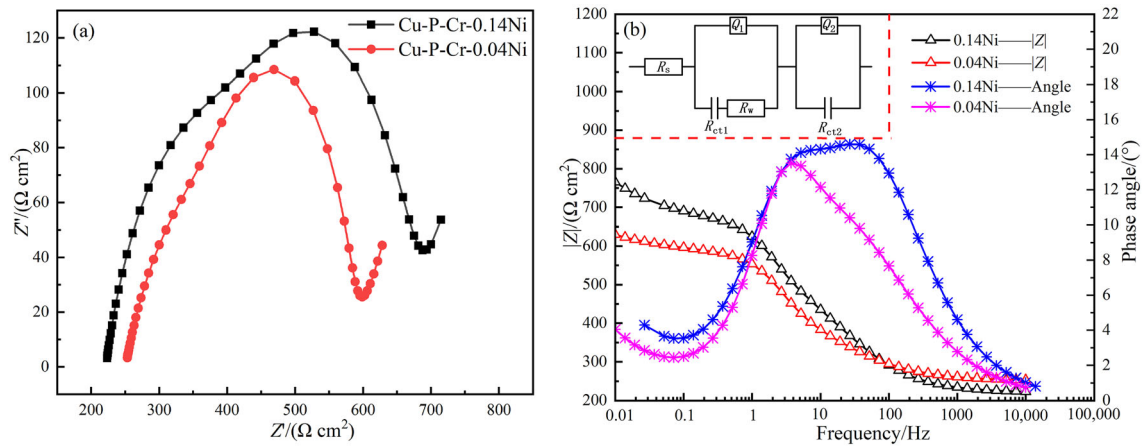


Fig. 6 Nyquist plots (a) and Bode plots (b) of bare steel

Table 4 Fitting results of parameters in equivalent circuit of bare steel

Steel	$R_s/(\Omega \text{ cm}^2)$	$Q_1/(\Omega^{-1} \text{ s}^n \text{ cm}^{-2})$	$R_{ct1}/(\Omega \text{ cm}^2)$	$R_w/(\Omega^{-1} \text{ s}^5 \text{ cm}^{-2})$	$Q_2/(\Omega^{-1} \text{ s}^n \text{ cm}^{-2})$	$R_{ct2}/(\Omega \text{ cm}^2)$
Cu–P–Cr–0.14Ni	221.8	$1.07 \times 10^{-4}$	223.0	0.0365	$4.512 \times 10^{-4}$	225.8
Cu–P–Cr–0.04Ni	250.9	$2.88 \times 10^{-4}$	180.6	0.0668	$4.515 \times 10^{-4}$	156.9

0.01 Hz ( $|Z|_{0.01}$ ) can be used to compare the corrosion resistance of the specimens. The larger the  $|Z|_{0.01}$ , the better the corrosion resistance of the specimen. It can be seen from Fig. 6b that  $|Z|_{0.01}$  value of Cu–P–Cr–0.14Ni steel was significantly higher than that of Cu–P–Cr–0.04Ni steel. The analysis results of Bode plots were in good accordance with that of polarization curve and Nyquist plots.

Figure 7b represents an equivalent electrical circuit model for EIS data fitting after periodic immersion corrosion test for 72 h [42], where  $R_r$  is rust layer resistance. Moreover, because the corrosion process of steel is controlled by diffusion of the elements, the Faraday impedance

is devised into two parts: the charge transfer resistance ( $R_t$ ) and  $R_w$ . The Nyquist plots of two tested steel after periodic immersion corrosion test for 72 h are shown in Fig. 7a. It can be seen that the diameter of arc in Nyquist plots of the two steels were similar. The plots were both composed of two curves in high frequency region and low frequency region, reflecting that they had similar anti-corrosion mechanism. The diameter of arc in the high frequency region reflected the electric double-layer between the outer rust layer and the solution, while the diameter of arc in the medium and low frequency region reflected the electric double-layer between the metal matrix and the infiltrated

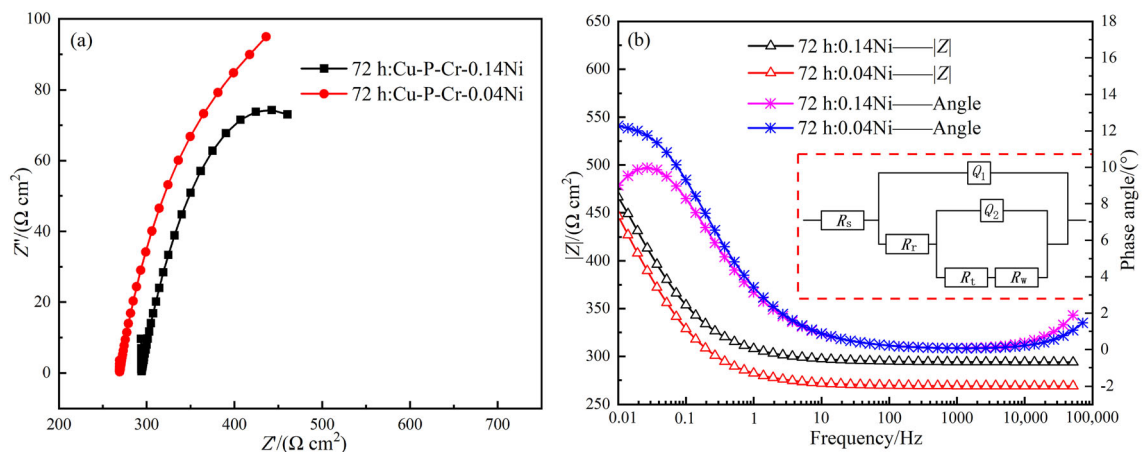


Fig. 7 Nyquist plots (a) and Bode plots (b) of tested steel after periodic immersion corrosion test for 72 h



electrolyte. The result also shows that the corrosion process was gradually controlled by electron transfer and diffusion process.

The Bode plots and phase angle plots of two tested steels after periodic immersion corrosion test for 72 h are shown in Fig. 7b. The resistance of rust layer can be used to evaluate the rust layer protective ability representing the barrier against migration of ions in association with the corrosion reaction. As shown in Fig. 7b, the low frequency region mainly reflected the charge transfer resistance between the rust layer and the substrate, while the high frequency region mainly reflected the rust layer resistance. It can be seen from Fig. 7b and Table 5 that the rust layer resistance, charge transfer resistance, and phase angle value of the two tested steels had little difference. The result shows that the rust layer protection abilities of the two tested steels were similar. Moreover, the result was consistent with XRD experimental results that  $\alpha$ -FeOOH content and  $\alpha/\gamma^*$  ratio of the two tested steels were similar.

### 3.6 Corrosion mechanism

In the initial stage of corrosion, the corrosion potential of Cu–P–Cr–0.14Ni steel and Cu–P–Cr–0.04Ni steel was  $-0.6852$  and  $-0.7037$  V, respectively. And then, the corrosion current density was  $2.8967 \times 10^{-5}$  and  $3.7705 \times 10^{-5}$  ( $\text{A cm}^{-2}$ ), respectively.  $|Z|_{0.01}$  value of Cu–P–Cr–0.14Ni steel was significantly higher than that of Cu–P–Cr–0.04Ni steel. Combining these results, the addition of Ni (0.14 wt.%) element increased the corrosion potential and decreased corrosion current density. And beyond that, the impedance value also increased greatly. However, the corrosion potential of Cu–P–Cr–0.14Ni steel and Cu–P–Cr–0.04Ni steel after periodic immersion corrosion test for 72 h was  $-0.6380$  and  $-0.6370$  V, respectively. Corrosion current density were  $2.0187 \times 10^{-5}$  and  $2.1316 \times 10^{-5}$  ( $\text{A cm}^{-2}$ ), respectively. And then,  $|Z|_{0.01}$  values of two tested steels were close. And beyond that, the mass loss rate of Cu–P–Cr–0.14Ni steel was  $1.57 \text{ g}/(\text{m}^2 \text{ h})$ , while the mass loss rate of Cu–P–Cr–0.04Ni steel was  $1.61 \text{ g}/(\text{m}^2 \text{ h})$ . It can also be found that the uniformity of corrosion products of the two tested steels was similar by observing the rust layer. The results of XRD experiment show that  $\alpha$ -FeOOH contents of the two tested steels were

$60.43\%$  and  $60.89\%$ , respectively. And then,  $\alpha/\gamma^*$  ratios were 1.53 and 1.56, respectively. Combining these results, there was no significant change after periodic immersion corrosion test for 72 h on the corrosion potential, impedance value and mass loss rate. In addition, the content of  $\alpha$ -FeOOH stable phase of two tested steels had little difference. In other words, the addition of Ni (0.14 wt.%) element only had an effect on the initial stage of corrosion. However, the effect was insignificant after periodic immersion corrosion test for 72 h. Zhou et al. [43] studied the corrosion behavior of Cr–Cu–0.5Ni low carbon steel and pointed out that the corrosion process could be divided into the initial stage in which the corrosion rate increased with accumulation of corrosion products and the later stage in which homogeneous and compact inner rust layers started to protect steel substrate out of corrosion mediums. The addition of Cr and Ni was beneficial to the formation of dense and compact inner rust layer, which was the most important reason for the improvement of corrosion resistance of experimental steel.

The following is the electrochemical reaction process of nickel [38]:

Anodic reaction



Adsorption of corrosion products



Transformation of rust crystals in the drying stage



The model of corrosion process is shown in Fig. 8. Figure 8 shows that the rust layers of two tested steels mainly consist of  $\text{Cr}_2\text{O}_3$ , CuO,  $\alpha$ -FeOOH,  $\gamma$ -FeOOH, and phosphate. The addition of Ni in Cu–P–Cr–0.14Ni steel produced NiO product. Li et al. [38] pointed out that a small amount of Ni mainly generated trace NiO that evenly distributed in the rust layers. With an increase in Ni content, more NiO were generated. A small amount of Ni ( $\leq 0.42$  wt.%) can significantly promote the crystallization of corrosion products and improve the stability of rust layer. In the initial stage of corrosion, Cu–P–Cr–0.14Ni steel surface quickly formed dense internal rust layer due to NiO that promoted the crystallization of corrosion products. However, the internal rust layer of Cu–P–Cr–0.04Ni steel was formed slowly and unevenly due to the extremely low Ni content. After periodic immersion corrosion test for 72 h, the role of Ni element was gradually weakened. It can be seen that there was no obvious difference in rust layer protection ability between the two tested steels. Remarkably, Cu and Cr elements were enriched in the inner rust layer, which existed in the form of CuO and  $\text{Cr}_2\text{O}_3$ , respectively. Therefore, the matrix was mainly protected

**Table 5** Fitting results of parameters in equivalent circuit of tested steel after periodic immersion corrosion test for 72 h

Steel	$R_f/(\Omega \text{ cm}^2)$	$R_t/(\Omega \text{ cm}^2)$
Cu–P–Cr–0.14Ni	293.8	284.7
Cu–P–Cr–0.04Ni	268.8	263.6

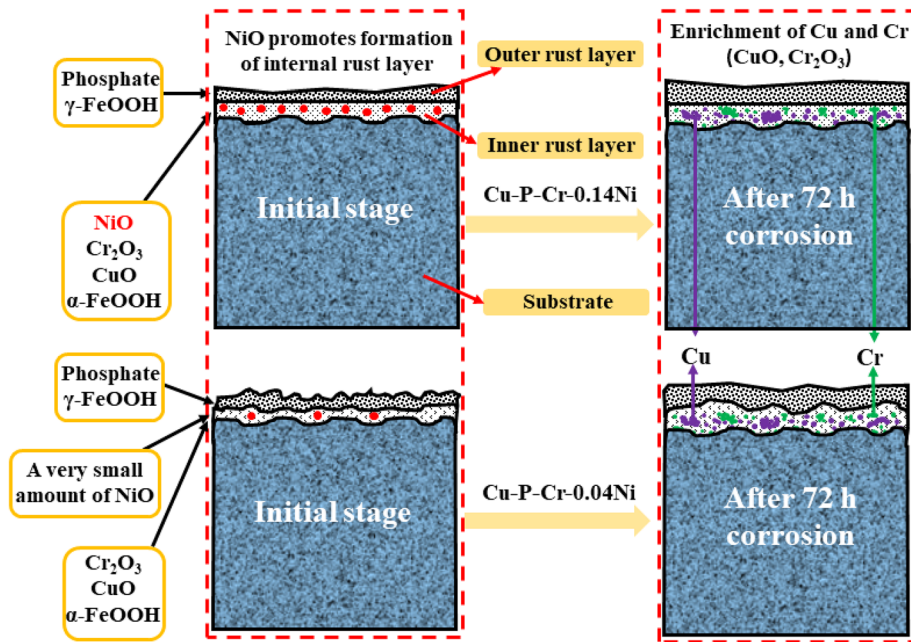


Fig. 8 Model of corrosion process

by  $\text{CuO}$  and  $\text{Cr}_2\text{O}_3$  after periodic immersion corrosion test for 72 h.

## 4 Conclusions

1. The mass loss rate of Cu–P–Cr–0.14Ni steel was  $1.57 \text{ g}/(\text{m}^2 \text{ h})$ , while the mass loss rate of Cu–P–Cr–0.04Ni steel was  $1.61 \text{ g}/(\text{m}^2 \text{ h})$ . The addition of Ni (0.14 wt.%) had no obvious effect on the mass loss rate after periodic immersion corrosion test for 72 h. The corrosion products of the two tested steels were mainly composed of  $\alpha$ -FeOOH,  $\gamma$ -FeOOH, and  $\beta$ -FeOOH.  $\alpha$ -FeOOH contents of the two tested steels were 60.43% and 60.89%, respectively. Ni element was evenly distributed in rust layer after periodic immersion corrosion test for 72 h. However, Cu and Cr elements were enriched in the inner rust layer, which existed in the form of  $\text{CuO}$  and  $\text{Cr}_2\text{O}_3$ , respectively.
2. The corrosion potential of the two tested steels at the initial stage of corrosion was  $-0.6852$  and  $-0.7037$  V, respectively. After periodic immersion corrosion test for 72 h, the corrosion potential of the two tested steels was  $-0.6380$  and  $-0.6370$  V, respectively. The corrosion potential difference between two tested steels with different Ni contents decreased gradually with the corrosion time reaching 72 h. In addition, the changes trend of impedance value was consistent with that of corrosion potential.
3. 0.14 wt.% Ni element had a significant effect on the improvement of corrosion potential and impedance

value at the initial stage of corrosion in Cu–P–Cr–0.14Ni steel. It was mainly in the form of NiO to promote the formation of a dense inner rust layer. However, the effect was insignificant after periodic immersion corrosion test for 72 h. The matrix was mainly protected by  $\text{CuO}$  and  $\text{Cr}_2\text{O}_3$ . Therefore, considering corrosion resistance and economy, low-nickel Cu–P–Cr weathering steel can be used.

**Acknowledgements** The authors appreciate the financial support from Maanshan Iron & Steel Co, Ltd. and Student Research Training Program of University of Science and Technology Beijing.

## References

- [1] R. Rihan, R. Shawabkeh, N. Al-Bakr, *J. Mater. Eng. Perform.* 23 (2014) 693–699.
- [2] J.F. Gu, Y. Xiao, N.W. Dai, X. Zhang, Q.Z. Ni, J.X. Zhang, *Corros. Eng. Sci. Technol.* 54 (2019) 249–256.
- [3] S. Sabir, A.A. Ibrahim, *Corros. Eng. Sci. Technol.* 52 (2017) 276–282.
- [4] W.Z. Wei, K.M. Wu, J. Liu, L. Cheng, X. Zhang, *J. Iron Steel Res. Int.* 28 (2021) 453–463.
- [5] T.Y. Zhang, W. Liu, Z. Yin, B.J. Dong, Y.G. Zhao, Y.M. Fan, J.S. Wu, Z. Zhang, X.G. Li, *J. Mater. Eng. Perform.* 29 (2020) 2531–2541.
- [6] D. de la Fuente, I. Díaz, J. Simancas, B. Chico, M. Morcillo, *Corros. Sci.* 53 (2010) 604–617.
- [7] I. Díaz, H. Cano, P. Lopesino, D. de la Fuente, B. Chico, J.A. Jiménez, S.F. Medina, M. Morcillo, *Corros. Sci.* 141 (2018) 146–157.
- [8] H. Cano, I. Díaz, D. de la Fuente, B. Chico, M. Morcillo, *Mater. Corros.* 69 (2018) 8–19.

- [9] Y.N. Niu, N. Dong, S. Liu, J. Yang, P.D. Han, Y.C. Wu, J. Iron Steel Res. Int. 28 (2021) 613–620.
- [10] Q.H. Zhao, W. Liu, J.W. Yang, Y.C. Zhu, B.L. Zhang, M.X. Lu, Int. J. Miner. Metall. Mater. 23 (2016) 1076–1086.
- [11] M. Kimura, H. Kihira, N. Ohta, M. Hashimoto, T. Senuma, Corros. Sci. 47 (2005) 2499–2509.
- [12] Y.H. Qian, C.H. Ma, D. Niu, J.J. Xu, M.S. Li, Corros. Sci. 74 (2013) 424–429.
- [13] Q.C. Zhang, J.S. Wu, J.J. Wang, W.L. Zheng, J.G. Chen, A.B. Li, Mater. Chem. Phys. 77 (2003) 603–608.
- [14] Z.L. Li, K. Xiao, C.F. Dong, X.Q. Cheng, W. Xue, W. Yu, J. Iron Steel Res. 26 (2019) 1315–1328.
- [15] Y.S. Choi, J.J. Shim, J.G. Kim, J. Alloy. Compd. 391 (2005) 162–169.
- [16] Y.G. Jia, C. Zhou, Y.H. Gao, Y. Zhou, M. Liu, H.X. Wang, J. Mater. Eng. Perform. 29 (2020) 1225–1234.
- [17] X.Q. Cheng, Z. Jin, M. Liu, X.G. Li, Corros. Sci. 115 (2017) 135–142.
- [18] H.Y. Ha, T.H. Lee, S.D. Kim, J.H. Jang, J. Moon, Metals 10 (2020) 891.
- [19] A. Tahara, T. Shinohara, Corros. Sci. 47 (2005) 2589–2598.
- [20] T. Mizoguchi, Y. Ishii, T. Okada, M. Kimura, H. Kihira, Corros. Sci. 47 (2005) 2477–2491.
- [21] W. Wu, Z.P. Zeng, X.Q. Cheng, X.G. Li, B. Liu, J. Mater. Eng. Perform. 26 (2017) 6075–6086.
- [22] T. Nishimura, H. Katayama, K. Noda, T. Kodama, Corros. Sci. 42 (2000) 1611–1621.
- [23] X.H. Chen, J.H. Dong, E.H. Han, W. Ke, Mater. Lett. 61 (2007) 4050–4053.
- [24] C.H. Song, X.J. Zhou, J.Z. Li, F. Huang, Z.H. Gan, R. Wu, Mater. Mech. Eng. 36 (2012) No. 4, 62–66+70.
- [25] T.W. Zhu, F. Huang, X.J. Zhou, J.Z. Li, Z.H. Lu, Corrosion & Protection 34 (2013) 963–966.
- [26] L.W. Xu, H.B. Li, H.B. Zheng, P.C. Lu, H. Feng, S.C. Zhang, W.C. Jiao, Z.H. Jiang, J. Iron Steel Res. Int. 27 (2020) 1466–1475.
- [27] J.Q. Jing, J. Guo, B. Li, S.J. Jia, Y. Ren, J. Iron Steel Res. Int. 28 (2021) 1037–1046.
- [28] C. Pan, M.X. Guo, W. Han, Z.Y. Wang, C. Wang, Corros. Eng. Sci. Technol. 54 (2019) 241–248.
- [29] Z.L. Li, K. Xiao, C.F. Dong, X.Q. Cheng, W. Xue, W. Yu, J. Iron Steel Res. Int. 26 (2019) 1315–1328.
- [30] Q.H. Zhao, W. Liu, Y.C. Zhu, B.L. Zhang, S.Z. Li, M.X. Lu, Acta Metall. Sin. (Engl. Lett.) 30 (2017) 164–175.
- [31] X.Q. Cheng, Y.W. Tian, X.G. Li, C. Zhou, Mater. Corros. 65 (2014) 1033–1037.
- [32] H. Cano, D. Neff, M. Morcillo, P. Dillmann, I. Diaz, D. de la Fuente, Corros. Sci. 87 (2014) 438–451.
- [33] Z.F. Wang, J.R. Liu, L.X. Wu, R.D. Han, Y.Q. Sun, Corros. Sci. 67 (2013) 1–10.
- [34] Y.Y. Chen, H.J. Tzeng, L.I. Wei, H.C. Shih, Mater. Sci. Eng. A 398 (2005) 47–59.
- [35] T. Kamimura, S. Hara, H. Miyuki, M. Yamashita, H. Uchida, Corros. Sci. 48 (2006) 2799–2812.
- [36] Q.F. Xu, K.W. Gao, Y.B. Wang, X.L. Pang, Appl. Surf. Sci. 345 (2015) 10–17.
- [37] J.H. Dong, E.H. Han, W. Ke, Sci. Technol. Adv. Mater. 8 (2007) 559–565.
- [38] D.L. Li, G.Q. Fu, M.Y. Zhu, Q. Li, C.X. Yin, Int. J. Miner. Metall. Mater. 25 (2018) 325–338.
- [39] Y.S. Choi, J.J. Shim, J.G. Kim, Corrosion 61 (2005) NACE-05050490.
- [40] Z.Y. Cui, X.G. Li, C. Man, K. Xiao, C.F. Dong, X. Wang, Z.Y. Liu, J. Mater. Eng. Perform. 24 (2015) 2885–2897.
- [41] W. Wu, W.K. Hao, Z.Y. Liu, X.G. Li, C.W. Du, W.J. Liao, J. Mater. Eng. Perform. 24 (2015) 4636–4646.
- [42] J. Guo, S.W. Yang, C.J. Shang, Y. Wang, X.L. He, Corros. Sci. 51 (2008) 242–251.
- [43] Y.L. Zhou, J. Chen, Y. Xu, Z.Y. Liu, J. Mater. Sci. Technol. 29 (2013) 168–174.